Structural and magnetic properties of Sb3+ ions doped Ni-Ba-Co ferrite prepared by sol-gel method

Yanchun Zhang
Northwest Normal University
Aimin Sun (sunam@nwnu.edu.cn)
Northwest Normal University https://orcid.org/0000-0002-1904-3153
Liqiong Shao
Northwest Normal University
Zhaxi Suonan
Northwest Normal University

Original Research

Keywords: Ni-Ba-Co ferrite, Sol-gel method, Sb3+ ions doped, Magnetic properties

Posted Date: February 12th, 2021

DOI: https://doi.org/10.21203/rs.3.rs-203610/v1

Version of Record: A version of this preprint was published at Journal of Materials Science: Materials in Electronics on April 3rd, 2021. See the published version at https://doi.org/10.1007/s10854-021-05799-5.

Structural and magnetic properties of Sb^{3+} ions doped Ni-Ba-Co ferrite prepared by sol-gel method

Yanchun Zhang[1], Aimin Sun[1,2 *], Liqiong Shao[1], Zhaxi Suonan[1]

1 College of Physics and Electronic Engineering, Northwest Normal University,

Lanzhou 730070, China

2 Key Laboratory of Atomic and Molecular Physics & Functional Materials of Gansu Province,

Lanzhou 730070, China

Abstract: In the present work, nanocrystalline Sb^{3+} ions doped $Ni_{0.2}Ba_{0.1}Co_{0.7}Fe_{2-x}Sb_xO_4$ ($0 \leqq x \leqq 0.1$, step by 0.025) ferrites were prepared via sol-gel method. The spinel-phase structure of samples can be confirmed by X-ray diffraction (XRD) patterns. The composition and structure were further studied by fourier transform infrared spectroscopy (FTIR). There were two typical characteristic bands ν_1 and ν_2 related to the stretching vibrations in spinel ferrite in FTIR spectra. Energy dispersive spectrometer (EDS) analyzed the elements of samples. It indicated that the elements of Ni, Ba, Co, Fe, O and Sb existed in the samples. Vibrating sample magnetometer was used to characterize magnetic properties. The saturation magnetization decreased from 57.65 emu/g to 44.50 emu/g with the increasing Sb^{3+} ions content, which is attributed to Fe^{3+} ions replaced by the Sb^{3+} ions. Remanent magnetization and coercivity first decreased and then increased slightly.

Keywords: Ni-Ba-Co ferrite; Sol-gel method; Sb^{3+} ions doped, Magnetic properties.

1. Introduction

In the past few decades, spinel ferrites have always attracted much attention due to largely considerable properties they appeared, such as spin glass behavior, magnetic compensation behavior, critical behavior, etc [1-3]. They have a wide range of applications covering industry, environment and bio-medicine, such as microwave communications [4], microwave absorbing material [5], adsorbents [6], catalysts [7], wastewater treatment [8], magnetic resonance imaging (MRI) [9], drug delivery and

* Corresponding Author: Aimin Sun AiminSun_1138@163.com

release [10]. The magnetic, optical and electronic properties of spinel ferrite nanoparticles are affected by many factors. The synthesis conditions and methods are critical factors. Some authors synthesize ferrite nanoparticles by various methods including co-precipitation [11], sonochemical approach [12], electrospinning method [13], sol-gel method [14], microemulsion method [15], thermal decomposition [16], etc. The conditions of pH and temperature also have effects on the morphology and magnetic properties of spinel ferrite [17-20]. Among a lot of prepared methods, sol-gel method has benefits of gathering safe, less economic consumption and short experiment period. The heat required in the process is provided by the reaction itself and does not require external supply, which is a key feature of sol-gel method [21]. The advantages of samples prepared this method are high purity, small uniform particle sizes and chemical homogeneity on an atomic scale. Among the many spinel ferrites, cobalt ferrite ($CoFe_2O_4$) has great coercivity and high magnetocrystalline and is suited to magnetic recording applications [22]. Barium ferrite ($BaFe_2O_4$) is rhombohedral and nonmagnetic material [23]. $NiFe_2O_4$ is a sort of soft ferrite regarded as a collinear ferrimagnet [24]. Ni-Ba-Co ferrite is one of the permanent magnetic material. Recently, modification of ferrite by chemical doping is a hot topic of research by scholars. Ashiq et al. [25] prepared $NiFe_{2-x}Sb_xO_4$ (x = 0.0, 0.2, 0.4, 0.6, 0.8 and 1) ferrite with the reverse microemulsion method and the crystallite size of samples were in the range of 8~38 nm. Anjum et al. [26] prepared $CdSb_xFe_{2-x}O_4$ (x=0.1, 0.2, 0.3, 0.4, 0.5) with the ceramic route and found that saturation magnetization decreased and coercivity increased with the increasing content of Sb^{3+} ions. Anjum et al. [27] also prepared $CoSb_{0.3}Fe_{1.7}O_4$ thin films via electron beam deposition technique. They found that the post annealing temperature is related to the growth of crystal structure. Lakshmi et al [28]. prepared Ni-Zn-Sb ferrite by hydrothermal method and found that the lattice parameter decreased with increasing content of antimony. There are no discovered literature on the properties of Sb^{3+} ions doped Ni-Ba-Co ferrite so far.

In this work, the $Ni_{0.2}Ba_{0.1}Co_{0.7}Fe_{2-x}Sb_xO_4$ ($0 \leqq x \leqq 0.1$, step by 0.025) ferrite were prepared with sol-gel method and citric acid was used as complexing agent. The complexing agents mainly play two roles in the experiment. One is to act as a

complexing agent to form a uniform and stable sol in the reaction process. Another is to act as a fuel for sol-gel auto-combustion. The effects of Sb^{3+} ions doped Ni-Ba-Co ferrite were explored.

2. Experimental Process

2.1 Materials

Cobalt nitrate [$Co(NO_3)_2 \cdot 6H_2O$] (Mw: 291.03 g/mol; 99%), ferric nitrate [$Fe(NO_3)_3 \cdot 9H_2O$] (Mw: 404.00 g/mol; 98.5%), nickel nitrate [$Ni(NO_3)_2 \cdot 6H_2O$], (Mw: 290.81 g/mol; 98%), antimony trioxide [Sb_2O_3], (Mw: 291.52 g/mol; 99.0%), barium nitrate [$Ba(NO_3)_2 \cdot 6H_2O$], (Mw: 261.34 g/mol; 99.5%), citric acid [$C_6H_8O_7 \cdot H_2O$], distilled water and ammonium hydroxide were used in this experiment to prepare the $Ni_{0.2}Ba_{0.1}Co_{0.7}Fe_{2-x}Sb_xO_4$ ($0 \leqq x \leqq 0.1$, step by 0.025) ferrite.

2.2 Synthesis

A series of Sb^{3+} ions doped Ni-Ba-Co ferrites have been prepared using sol-gel method having the general formula $Ni_{0.2}Ba_{0.1}Co_{0.7}Fe_{2-x}Sb_xO_4$ ($0 \leqq x \leqq 0.1$, step by 0.025). The preparation of the sample includes some processes which are shown in Fig. 1. Nitrates weighed in stoichiometric ratio and citric acid at the molar ratio of 1:1.2 mixed in 100 mL distilled water. After the solute is completely dissolved, ammonium hydroxide is used to adjust the pH=7 under the condition of uniform stirring. The precursor solution was heated at 80 ℃ for 3h in magnetic heating and stirring agitator. Then the solution turned to a wet sol. The wet sol was put in dry blast oven at 120 ℃ for 2 h to form a dry gel. The dry gel was heated with an alcohol lamp. The obtained floccule was ground about 1 h until it forms black powder. The powders were annealed in muffle furnace at 1100 ℃ for 2 h. The obtained powders were ground about 20 min to obtain final samples.

2.3 Characterization techniques

The XRD patterns were collected by Germany Bruch diffractometer with a goniometer using Cu-Kα radiation ($\lambda = 0.15406$ nm). The diffracted intensities were recorded in the angular range 20~80°. The infrared absorption spectra of samples were recorded by fourier transform infrared spectroscopy (China WQF-510). The morphology and shape of samples were observed by scanning electron microscopy (Japan JSM-6700F). The magnetic measurements were obtained by

vibrating sample magnetometer (USA Lakeshore 7304).

3. Results and discussion

3.1 Structural properties

The lattice structure of spinel ferrite belongs to face-centered cubic (space group Oh7-F3dm) and is densely packed with O^{2-}, cations fill the gaps where the O^{2-} are densely packed. In the face-centered cubic lattice constituted by the accumulation of 32 O^{2-}, there are two kinds of gaps, namely tetrahedral A site and octahedral B site. The crystal structure and the distribution of cations and O^{2-} of spinel ferrite are shown in Fig.2. The overlapping area among the electron cloud of each magnetic ion is inexistent. The magnetism is generated by the superexchange of nonmagnetic O^{2-} as media. The exchange interaction at A-B is the strongest. Figure 3 shows the relative positions of cation and O^{2-} in the superexchange of ferrite.

Figure 4 shows X-ray diffraction pattern of the pure and Sb^{3+} ions doped $Ni_{0.2}Ba_{0.1}Co_{0.7}Fe_2O_4$ ferrite samples. It can be observed from Fig.4 that the pure $Ni_{0.2}Ba_{0.1}Co_{0.7}Fe_2O_4$ ferrite has the diffraction peaks of (220), (311), (222), (400), (422), (511) and (440), which indicates the formation of spinel structure. Whereas Sb^{3+} ions doped samples show additional peaks besides spinel when x > 0.075, which may be related to secondary phase. When the doping content increases, Sb^{3+} ions do not enter the lattice, but enriched at the grain boundary to form Sb_2O_3 phase. The lattice constant (a) can be calculated by the relation [29]:

$$a = d\sqrt{h^2 + k^2 + l^2} \tag{1}$$

Where (h k l) are Miller index, ‘d’ is inter planar spacing. The average crystallite size (D) can be calculated by the Scherrer’s formula. The formula is as follows [30]:

$$D = \frac{0.9\lambda}{\beta \cos\theta} \tag{2}$$

Where 0.9 is shape factor, ‘β’ is the full width at half maximum of the diffraction angle. The values of lattice constant (a) and average crystallite sizes (D) are shown in Table 1. It is clear from Fig.5 that lattice constant first decreases from 8.3625 Å to 8.3562 Å and then increases with the increasing Sb^{3+} ions content. The reason for the decrease of lattice constant is that Sb^{3+} ion (0.76 Å) may be oxidized to Sb^{5+} ion (0.60 Å) when samples were annealed at 1100~1200 ℃ [31]. The Sb^{5+} ions with smaller

ionic radius are accommodated on the lattice by replacing Fe^{3+} ion (0.67 Å). The increased phenomenon of lattice constant can be related to cation redistribution and bigger ionic radius of Sb^{3+} ion (0.76 Å) when the content of Sb^{3+} ions further increased. The average crystallite sizes of prepared samples decreased from 29.37 nm to 22.07 nm. The decrease in average crystallite sizes may be due to energy consumption when Sb^{3+} ions enter into the lattice [32]. The dislocation linear density (δ) can be calculated by the formula:

$$\delta = \frac{1}{D^2} \tag{3}$$

The X-ray density (ρ_x) can be calculated by the formula [33]:

$$\rho_x = \frac{8M}{N_A a^3} \tag{4}$$

Where 'M' represents the molecular mass; 'a^3' is volume of unit cell; 'N_A' is the Avogadro's constant and the value is 6.02214076×10^{23} mol^{-1}. The values of dislocation linear density and X-ray density of samples are shown in Table 1. The X-ray density of samples increased with the increasing content of Sb^{3+} ions. That is due to the replacement of Fe^{3+} (55.85 g/mol) by Sb^{3+} having a bigger molecular mass (121.76 g/mol).

3.2 FTIR spectroscopic analysis

FTIR was performed to discover the the position and valence of ions in the crystal lattice of Sb^{3+} ions doped Ni-Ba-Co ferrite. FTIR spectra at room temperature of $Ni_{0.2}Ba_{0.1}Co_{0.7}Fe_{2-x}Sb_xO_4$ ($0 \leqq x \leqq 0.1$, step by 0.025) are shown in Fig.6. M-O band in tetrahedral A site is related to the higher force constants and lower bond lengths, so the stretching vibration frequency between M-O at A site may locate near higher band. The lower band is attributed to the stretching vibration of M-O in octahedral B site [34]. From Fig.6, it can be observed that the two absorption bands ν_1 around 600 cm^{-1} and ν_2 near 400 cm^{-1} are clear. The frequency values ν_1 and ν_2 are shown in Table 2. The appearance of two bands prove that the spinel structure of the prepared samples. With the increasing content of Sb^{3+} ions, the ν_1 moves to lower frequency from 613 cm^{-1} to 603 cm^{-1}. It indicates that Sb^{3+} ions replace Fe^{3+} ions into lattice, thereby

causing the change of bond length. Some small absorption bands are observed in the Fig.6. The band near 1641 cm^{-1} may be attributed to the stretching vibration of -OH in adsorbed molecular water [35]. The band around 1388 cm^{-1} is seen as the vibration of anti-symmetric NO_3^- bond, the decrease or disappearance of the band at 1388 cm^{-1} can indicate that NO_3^- participated in the process of reaction [36]. The band located at 1091 cm^{-1} may be related to the stretching vibration of residual C-O bond.

3.3 SEM and chemical elements analysis

The morphological micrographs of the prepared $Ni_{0.2}Ba_{0.1}Co_{0.7}Fe_{2-x}Sb_xO_4$ ($0 \leqq x \leqq 0.1$, step by 0.025) ferrite annealed at 1100 ℃ are displayed in Fig.7. Figure 7 show the varying degrees of agglomeration with the increasing content of Sb^{3+} ions. The agglomeration appears among particles due to the magnetic dipole-dipole interactions along with Van der Waals force [37]. It indicates that every particles are composed of a lot of small grains. Energy dispersive spectrometer is used to analyze elements and ingredients of prepared samples. The EDS diagrams are displayed in Fig.8. It can be confirmed that there are five elements in pure sample, which are Ni, Ba, Co, Fe and O. It can be observed that the existence of Sb element in doped samples besides the above five main elements.

3.4 Magnetic properties

The magnetic characterization of $Ni_{0.2}Ba_{0.1}Co_{0.7}Fe_{2-x}Sb_xO_4$ ($0 \leqq x \leqq 0.1$, step by 0.025) is recorded at room temperature. The hysteresis loop of the prepared samples is shown in Fig.9. Values of coercivity (Hc), remanent magnetization (Mr), saturation magnetization (Ms) are shown in Table 3. It shows from hysteresis loops that samples are typical hard ferromagnetic materials. The variations of remanent magnetization and saturation magnetization with the increasing of Sb^{3+} ions are shown in Fig.10(a). *Ms* decreased from 57.65 emu/g to 44.50 emu/g, *Mr* first decreased from 25.66 emu/g to 13.88 emu/g and then increased from 13.88 emu/g to 15.03 emu/g. The magnetic properties of spinel ferrite mainly come from metal cation superexchange between A and B sites. Ni^{2+} ions ($2\mu_B$) are known to have a preference for the B site, Co^{2+} ions ($3\mu_B$) and Fe^{3+} ions ($5\mu_B$) occupy A site and B site in most cases. Sb^{3+} ($0\mu_B$) ions have a strong B site preference [25]. According to Néel ferromagnetic theory, the ions in the A and B sites spontaneously magnetize in opposite directions and the

magnetization are not equal and can not completely offset. The remaining spontaneous magnetization appears. The net magnetic moment (M) of a unit cell can be described as $M = M_B - M_A$, M_B and M_A represent the magnetic moment of B site and A site, respectively [38]. Due to the partial replacement of magnetic ions (Fe^{3+}) with Sb^{3+} (non-magnetic ions), the magnetization of B site decreased, which weakens superexchange A-B. Accordingly, saturation magnetization decreased. For spinel ferrite, the Bohr magnetic moment can be calculated by the formula [39]:

$$\mu_B(\exp.) = \frac{M_W \times M_S}{5585} \tag{5}$$

Where 'M_W' is the molecular weight. The value of unit cell magnetic moment μ_B(exp.) is shown in Table 4. The demagnetization curve located in the second quadrant of the hysteresis loop is an important basis for examining the hard magnetic materials. The coercivity is the strength of the reverse magnetic field that needs to be applied to reduce the magnetization of the magnetized magnet to 0. The coercivity decreased from 952.31 Oe to 800.68 Oe when the content of Sb^{3+} ions increased up to x=0.075, then the coercivity slightly increased from 800.68 Oe to 844.35 Oe. A similar phenomenon occurs in the reference [26], the coercivity first decreased and then increased with the increasing content of Sb^{3+} ions in $CdSb_xFe_{2-x}O_4$ series ferrites. Anisotropy constant (K) can be estimated by the following formula [40]:

$$K = \frac{1}{2}\mu_0 H_C M_S \tag{6}$$

Where 'μ_0' is magnetic permeability in vacuum (equal to 1 in Gauss unit system). The value of anisotropy constant is displayed in Table 4. From Fig.10(b), it can be observed that 'K' decreased with the increasing content of Sb^{3+} ions. The value of squareness S (Mr/Ms) and coercivity squareness (S^*) can be seen in Table 3, which is a significant parameter about anisotropy. The value of S are 0.445, 0.412, 0.313, 0.320 and 0.338, respectively. These values are less than 0.5, which indicate the presence of multi-domain (MD) state, pseudo-single domain (PSD) state and single domain (SD) state. The magnetization and the external magnetic field have the following relationship:

$$M = \chi H \tag{7}$$

Where 'χ' is magnetic susceptibility. Magnetic susceptibility 'χ' can be expressed by

the field dependence of dM/dH curves, which characterize the feature of domain about prepared samples. The field dependence of dM/dH curves of prepared $Ni_{0.2}Ba_{0.1}Co_{0.7}Fe_{2-x}Sb_xO_4$ ($0 \leqq x \leqq 0.1$, step by 0.025) are shown in Fig.11. As far as an ideal single domain particle is concerned, the value of dM/dH at $H \rightarrow 0$ is 0 [41,42]. The dM/dH values of samples at $H \rightarrow 0$ is 18.57, 19.76, 16.76, 18.89 and 16.98 in 10^{-3} emu/g Oe, respectively. It indicates further that the prepared samples have multi-domain particles. The dM/dH values at $H \rightarrow H_m$ are shown in Table 4. The higher peak height of dM/dH at Hm is, the better crystalline cubic spinel structure the samples have. It indicates that the $Ni_{0.2}Ba_{0.1}Co_{0.7}Fe_2O_4$ sample has a magnetically stable state.

4. Conclusions

The sol-gel method was used to prepare $Ni_{0.2}Ba_{0.1}Co_{0.7}Fe_{2-x}Sb_xO_4$ ($0 \leqq x \leqq 0.1$, step by 0.025) ferrites, citric acid acted as complexing agent and fuel for auto-combustion. The XRD, FTIR, SEM, EDS and VSM were used to characterize the samples. The samples have spinel structure. The lattice constant first decreases and then increases. The average crystallite sizes of prepared samples are in the range of 29.37~22.07 nm. The SEM imagines show the varying degrees of agglomeration among particles, which can be attributed to magnetostatic coupling between the particles. Due to the replacement of magnetic ions (Fe^{3+}) with Sb^{3+} ions, the magnetic properties (Ms, Mr and Hc) are all less than these of $Ni_{0.2}Ba_{0.1}Co_{0.7}Fe_2O_4$ sample with the increasing content of Sb^{3+} ions. The values of Mr/Ms (S) are less than 0.5, which indicate the presence of multi-domain (MD) state, single domain (SD) state and pseudo-single domain (PSD) state in samples.

Author contributions

Yanchun Zhang: contributed to experiment, conceptualization, investigation, writing-original draft and visualization; Aimin Sun: checked the manuscript; Liqiong Shao : checked the table and Nanzhaxi Suo: helped in measurement of data,experimental process, checking the figure.

Additional Information

Competing financial interests: The authors declare no competing financial interests.

Supplementary information: The authors claim that none of the material in the paper has been published or is under consideration for publication elsewhere.

References

[1] Chaocheng Liu, Xucai Kan, Xiansong Liu, Zhitao Zhang and Jiyu Hu. Magnetic compensation and critical behavior in spinel Co_2TiO_4. Phys. Chem. Chem. Phys.

[2] Wei Yang, Xucai Kan, Xiansong Liu, Zhongzhu Wang, Zuhua Chen, Zhen Wang, Ruiwei Zhu, Mudssir Shezad. Spin glass behavior in $Zn_{0.8-x}Ni_xCu_{0.2}Fe_2O_4$ ($0 \leqq x \leqq 0.28$) ferrites. Ceram. Int. 45 (2019) 23328-23332.

[3] Yong Li, Xucai Kan, Xiansong Liu, Shuangjiu Feng, Qingrong Lv, Khalid Mehmood Ur Rehma, Wei Wang, Chaocheng Liu, Xiaohui Wang, Yuliang Xu. Spin-glass evolution behavior in spinel compounds $Co_{2-x}Zn_xSnO_4$ ($0 \leqq x \leqq 1$). J. Alloy. Compd.

[4] T. Alves, R. Augustine, P. Que´ffe´lec, M. Grzeskowiak, B. Poussot and J.-M. Laheurte. Polymeric ferrite-loaded antennas for on-body communications. Microwave and Optical technology Letters / Vol. 51, No. 11, November 2009.

[5] Abdülhadi Baykal, Nermin Kasapoğlu, Yüksel Köseoğlu, Ali Cemil Başaran, Hüseyin Kavas, Muhammet S.Toprak. Microwave-Induced Combustion Synthesis and Characterization of $Ni_xCo_{1-x}Fe_2O_4$ Nanocrystals (x = 0.0, 0.4, 0.6, 0.8, 1.0). Cent. Eur. J. Chem. 6 2008 125-130.

[6] Jinbo Wei, Xiaofei Zhang, Qi Liu, Zhanshaung Li, Lianhe Liu, Jun Wang. Magnetic separation of uranium by $CoFe_2O_4$ hollow spheres. Chemical Engineering Journal 241 (2014) 228−234.

[7] Kula Kamal Senapati, Chandan Borgohain, Prodeep Phukan. Synthesis of highly stable $CoFe_2O_4$ nanoparticles and their use as magnetically separable catalyst for Knoevenagel reaction in aqueous medium. Journal of Molecular Catalysis A: Chemical 339 (2011) 24-31.

[8] K.K. Kefeni, B.B. Mamba, T.A.M. Msagati, Application of spinel ferrite nanoparticles in water and wastewater treatment: A review, Separation and Purification Technology (2017).

[9] Xingjun Zhu, Jing Zhou, Min Chen, Mei Shi, Wei Feng, Fuyou Li. Coreeshell Fe_3O_4@NaLuF4:Yb,Er/Tm nanostructure for MRI, CT and upconversion luminescence tri-modality imaging. Biomaterials 33 (2012) 4618-4627.

[10] Alireza Meidanchi, Omid Akhavan, Samideh Khoei, Ali A. Shokri, Zahra Hajikarimi, Nakisa Khansari. $ZnFe_2O_4$ nanoparticles as radiosensitizers in radiotherapy of human prostate cancer cells.

[11] S. Amiri, H. Shokrollahi. Magnetic and structural properties of RE doped Co-ferrite (RE=Nd, Eu, and Gd) nano-particles synthesized by co-precipitation. Journal of Magnetism and Magnetic Materials 345 (2013) 18−23.

[12] M.A. Almessiere, Y. Slimani, A.D. Korkmaz, S. Guner, M. Sertkol, S.E. Shirsath, A.Baykal, Structural, optical and magnetic properties of Tm^{3+} substituted cobalt spinel ferrites synthesized via sonochemical approach, Ultrasonics Sonochemistry (2019).

[13] Montana Sangmanee, Santi Maensiri. Nanostructures and magnetic properties of cobalt ferrite (CoFe2O4) fabricated by electrospinning. Appl Phys A (2009) 97: 167–177.

[14] Thomas Dippong, Erika Andrea Levei, Iosif Grigore Deac, Emilia Neag and Oana Cadar. Influence of Cu^{2+}, Ni^{2+}, and Zn^{2+} Ions Doping on the Structure, Morphology, and Magnetic Properties of Co-Ferrite Embedded in SiO_2 Matrix Obtained by an Innovative Sol-Gel Route. Nanomaterials 2020, 10, 580.

[15] V.Pillai, D.O. Shah.Synthesis of high-coercivity cobalt ferrite particles using water-in-oil microemulsions. J. Magn. Magn. Mater.163 (1996) 243-248.

[16] Marcela Stoia, Paul Barvinschi, Lucian Barbu Tudoran, Mirela Barbu, Mircea Stefanescu. Synthesis of nanocrystalline nickel ferrite by thermal decomposition of organic precursors. J Therm Anal Calorim (2012) 108:1033−1039.

[17] K.H. Wu, W.C. Huang, G.P. Wang, T.R. Wu. Effect of pH on the magnetic and dielectric properties of SiO_2/NiZn ferrite nanocomposites. Materials Research Bulletin 40 (2005) 1822-1831.

[18] Manish Srivastava, Animesh K. Ojha, S. Chaubey, Prashant K. Sharma, Avinash C. Pandey. Influence of pH on structural morphology and magnetic properties of ordered phase cobalt doped lithium ferrites nanoparticles synthesized by sol-gel method. Materials Science and Engineering B 175 (2010) 14-21.

[19] K. Maaz, S. Karim, Kyu Joon Lee, Myung-Hwa Jung, Gil-Ho Kim. Effect of temperature on the magnetic characteristics of $Ni_{0.5}Co_{0.5}Fe_2O_4$ nanoparticles. Materials Chemistry and Physics 133 (2012) 1006-1010.

[20] E. Ranjith Kumar, R. Jayaprakash. Effect of combustion rate and annealing temperature on structural and magnetic properties of manganese substituted nickel and zinc ferrites. Journal of Magnetism and Magnetic Materials 348 (2013) 93-100.

[21] A.C.F.M. Costa, E. Tortella, M.R. Morelli, R.H.G.A. Kiminami. Synthesis, microstructure and magnetic properties of Ni-Zn ferrites. J. Magn. Magn. Mater. 256 (2003) 174−182.

[22] C.H. Chia, S. Zakaria, M. Yusoff, S.C. Goh, C.Y. Haw, Sh. Ahmadi, N.M. Huang, H.N. Lim. Size and crystallinity-dependent magnetic properties of $CoFe_2O_4$ nanocrystals. Ceramics International 36 (2010) 605-609.

[23] Warren B. Cross, Louise Affleck, Maxim V. Kuznetsov, Ivan P. Parkin and Quentin A. Pankhurst, Self-propagating high-temperature synthesis of ferrites MFe_2O_4 (M= Mg, Ba, Co, Ni, Cu, Zn); reactions in an external magnetic field. J. Mater. Chem., 1999, 9, 2545-2552.

[24] U. V. CHHAYA, B. S. TRIVEDI, R. G. KULKARNI, Magnetic ordering and properties of nickel ferrite doped with Al^{3+} and Cr^{3+} ions. Journal of Materials Science Letters 18 (1 9 9 9) 1177 –1179.

[25] Muhamamd Naeem Ashiq, Muhammad Fahad Ehsan, Muhammad Javed Iqbal, Iftikhar Hussain Gul. Synthesis, structural and electrical characterization of Sb^{3+} substituted spinel nickel ferrite ($NiSb_xFe_{2-x}O_4$) nanoparticles by reverse micelle technique. Journal of Alloys and Compounds 509 (2011) 5119–5126.

[26] Safia Anjum, Tafruj Ilayas, Zeeshan Mustafa. Infuence of antimony substitution on structural, magnetic and optical properties of cadmium spinel ferrite. Applied Physics A (2020) 126:227.

[27] Safia Anjum, Asmara Shabab, Shahid Rafifique, Rehana Zia, Saira Riaz, Sania Hameed, Madeeha Riaz. Crystal growth of antimony substituted cobalt ferrites thin films deposited by electron beam. Optik 127 (2016) 8487–8498.

[28] Ch.S. Lakshmi, Ch.S.L.N. Sridhar, G. Govindraj, S. Bangarraju, D.M. Potukuchi. Structural, magnetic and dielectric investigations in antimony doped nano-phased nickel-zinc ferrites. Physica B 459 (2015) 97-104.

[29] J.S. Ghodake, Rahul C. Kambale, T.J. Shinde, P.K. Maskar, S.S. Suryavanshi. Magnetic and microwave absorbing properties of Co^{2+} substituted nickel–zinc ferrites with the emphasis on initial permeability studies. Journal of Magnetism and Magnetic Materials 401 (2016) 938–942.

[30] Le-Zhong Li, Zhong Yu, Zhong-Wen Lan, Ke Sun, Chuan-Jian Wu. Structural and magnetic properties of Mg-substituted NiZnCo ferrite nanopowders. Ceramics International (2014).

[31] M. A. Tena, S. Sorlı´, M. Llusar, J. A. Badenes, A. Fore´s, and G. Monro´s. Study of Sb-doped SnO_2 Gray Ceramic Pigment with Cassiterite Structure. Z. Anorg. Allg. Chem. 2005, 631, 2188-2191.

[32] Chandan C. Naik, A.V. Salker. Effect of fractional substitution of Sb^{3+} ions on structural, magnetic and electrical properties of cobalt ferrite. Materials Science & Engineering B 258 (2020) 114574.

[33] P.A. Shaikh, R.C. Kambale, A.V. Rao, Y.D. Kolekar. Effect of Ni doping on structural and magnetic properties of $Co_{1-x}Ni_xFe_{1.9}Mn_{0.1}O_4$. Journal of Magnetism and Magnetic Materials 322 (2010) 718–726.

[34] Kumar Mohit, Vibha Rani Gupta, Nisha Gupta, S.K. Rout. Structural and microwave characterization of $Ni_{0.2}Co_xZn_{0.8-x}Fe_2O_4$ for antenna applications. Ceramics International 40 (2014) 1575-1586.

[35] Wei Zhang , Aimin Sun, Xiqian Zhao , Xiaoguang Pan , Yingqiang Han , Nanzhaxi Suo , Lichao Yu , Zhuo Zuo. Structural and magnetic properties of Ni-Cu-Co ferrites prepared from sol-gel auto combustion method with different complexing agents. J. Alloy. Compd. 816 (2020) 152501.

[36] K.H. Wu, T.H. Ting, C.C. Yang, G.P.Wang. Effect of complexant/fuel on the chemical and electromagnetic properties of SiO_2-doped Ni-Zn ferrite. Materials Science and Engineering B 123 (2005) 227–233.

[37] Mritunjoy Prasad Ghosh, Pramanand Kumar, Manoranjan Kar, and Samrat Mukherjee. Impact of In^{3+} ion substitution on microstructural, magnetic and dielectric responses of nickel-cobalt spinel ferrite nanocrystals. J Mater Sci: Mater Electron.

[38] K. Kumar, A. Loganathan. Structural, electrical and magnetic properties of large ionic size Sr^{2+} ions substituted Mg-Ferrite nanoparticles. Materials Chemistry and Physics 214 (2018) 229-238.

[39] Sagar E. Shirsath, Mahesh L. Mane, Yukiko Yasukawa, Xiaoxi Liu and Akimitsu Morisako. Self-ignited high temperature synthesis and enhanced super-exchange interactions of Ho^{3+}-Mn^{2+}-Fe^{3+}-O^{2-} ferromagnetic nanoparticles. Phys. Chem. Chem. Phys. 2014, 16, 2347.

[40] Nanzhaxi Suo, Aimin Sun, Lichao Yu, Zhuo Zuo, Xiqian Zhao, Wei Zhang, Yanchun Zhang, Liqiong Shao, Tengxuan Yu. Preparation and study of lattice structure and magnetic properties of Bi^{3+} ion-doped Ni-Mg-Co ferrites by sol-gel auto-combustion method. Journal of Sol-Gel Science and Technology.

[41] I. Panneer Muthuselvam, R.N. Bhowmik. Mechanical alloyed Ho^{3+} doping in $CoFe_2O_4$ spinel ferrite and understanding of magnetic nanodomains. J. Magn Magn Mater 322 (2010) 767–776.

[42] N. Dipesh, L. Wang, H. Adhikari, J. Alam, S.R. Mishra, Influence of Al^{3+} doping on structural and magnetic properties of $CoFe_{2-x}Al_xO_4$ Ferrite nanoparticles, Journal of Alloys and Compounds (2016).

Figures

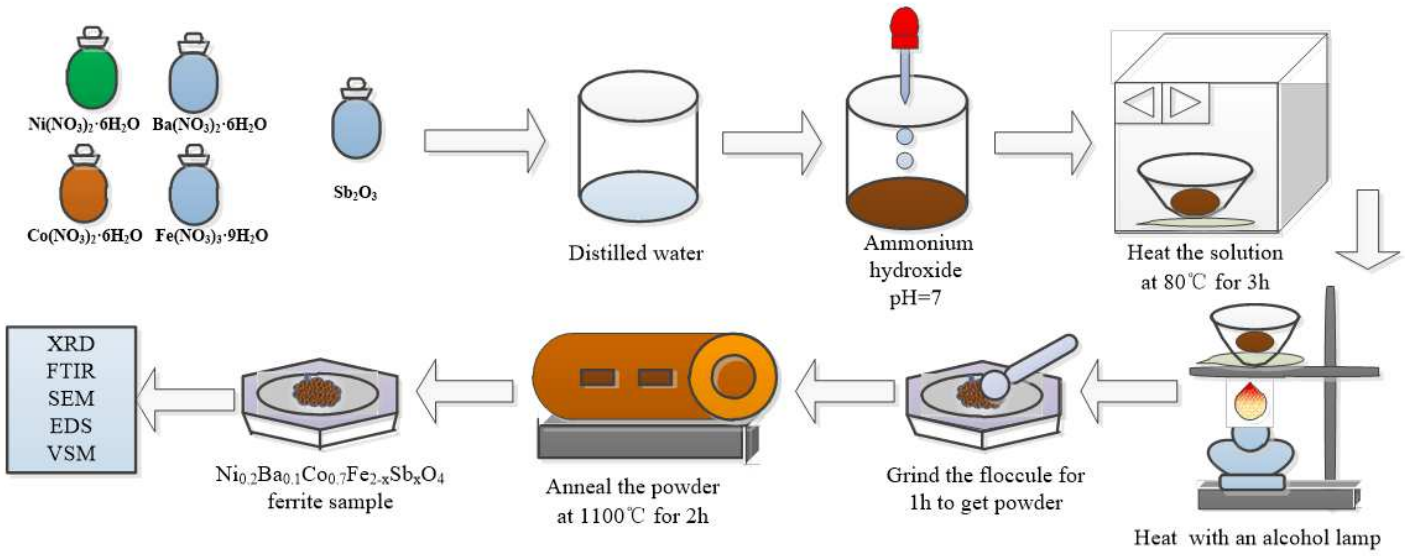

Figure 1

The flow chart of preparing Ni0.2Ba0.1Co0.7Fe2-xSbxO4 (x=0, 0.025, 0.05, 0.075 and 0.1) ferrite by sol-gel method.

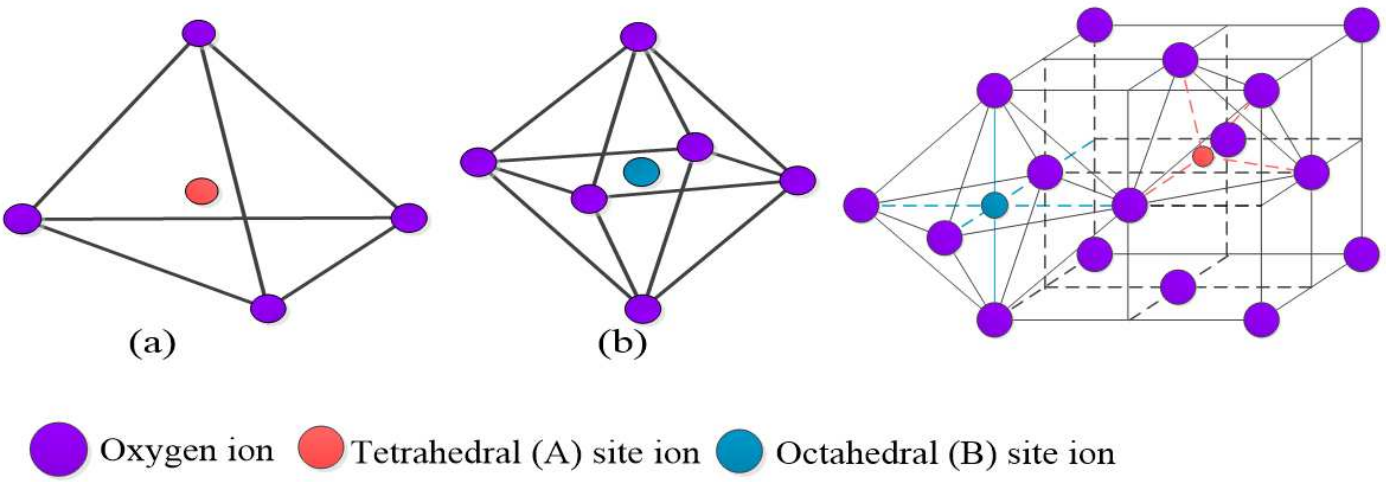

Figure 2

The crystal structure of spinel ferrite and the distribution of metal cations and oxygen ions. (a) Tetrahedral A site; (b) Octahedral B site.

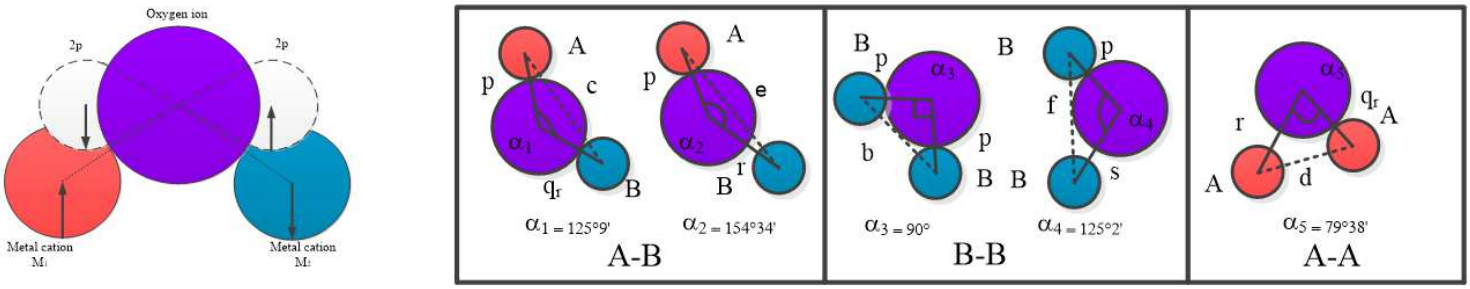

Figure 3

The relative positions of metal ions and oxygen ions in the superexchange of spinel ferrite.

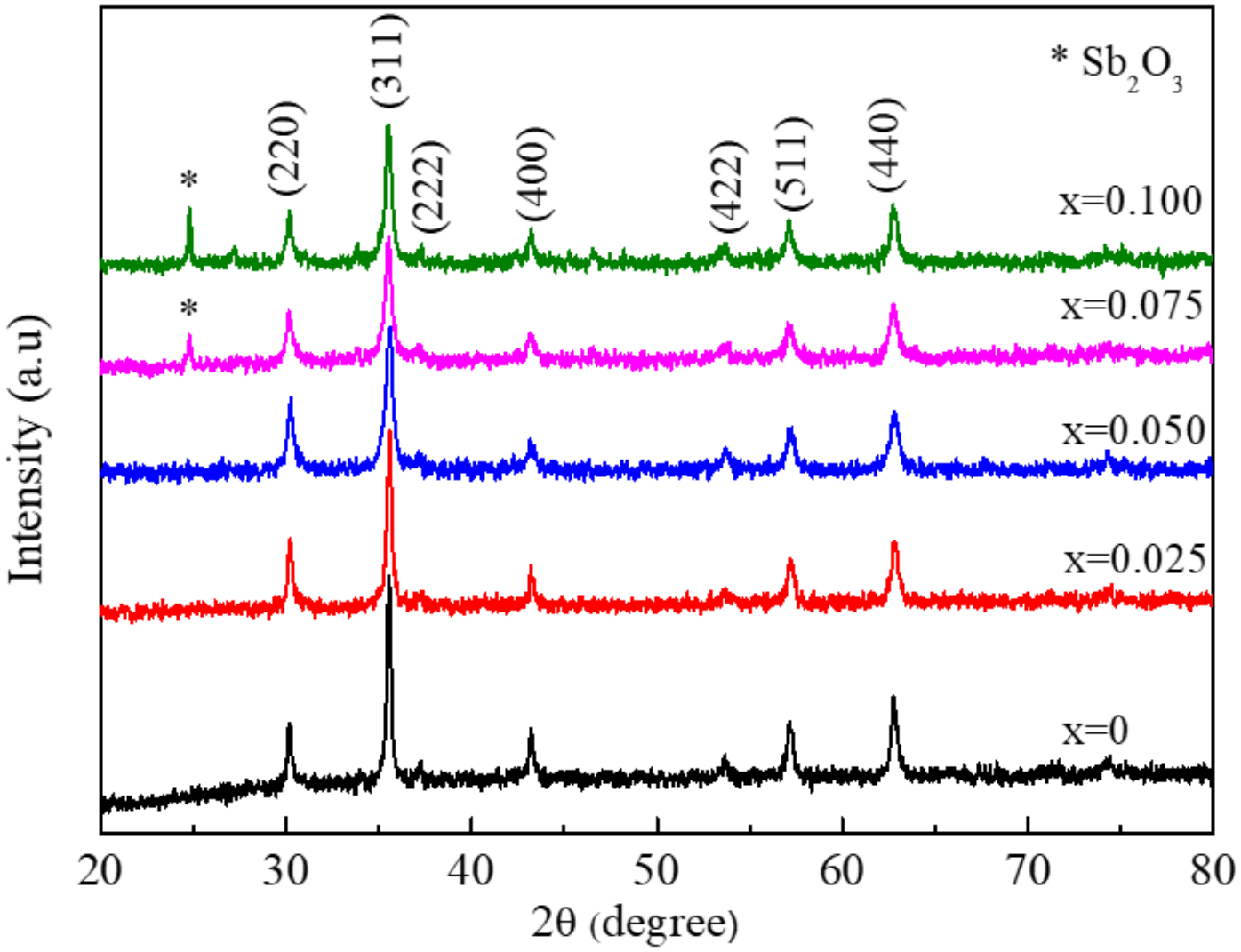

Figure 4

The X-ray diffraction pattern of Ni0.2Ba0.1Co0.7Fe2-xSbxO4 (x=0, 0.025, 0.05, 0.075 and 0.1) nano ferrite.

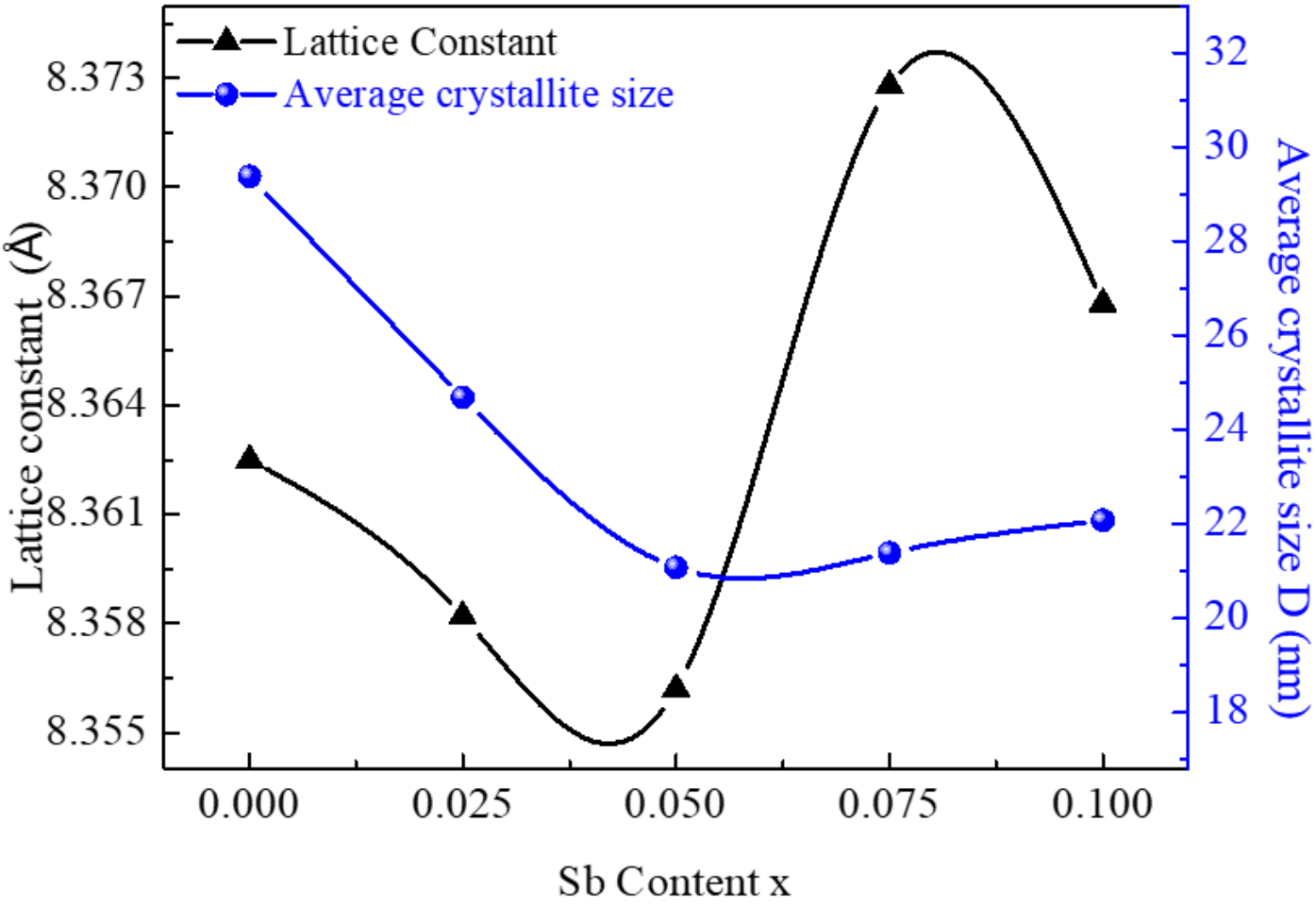

Figure 5

Variation of lattice constant, average crystallite size Sb content x.

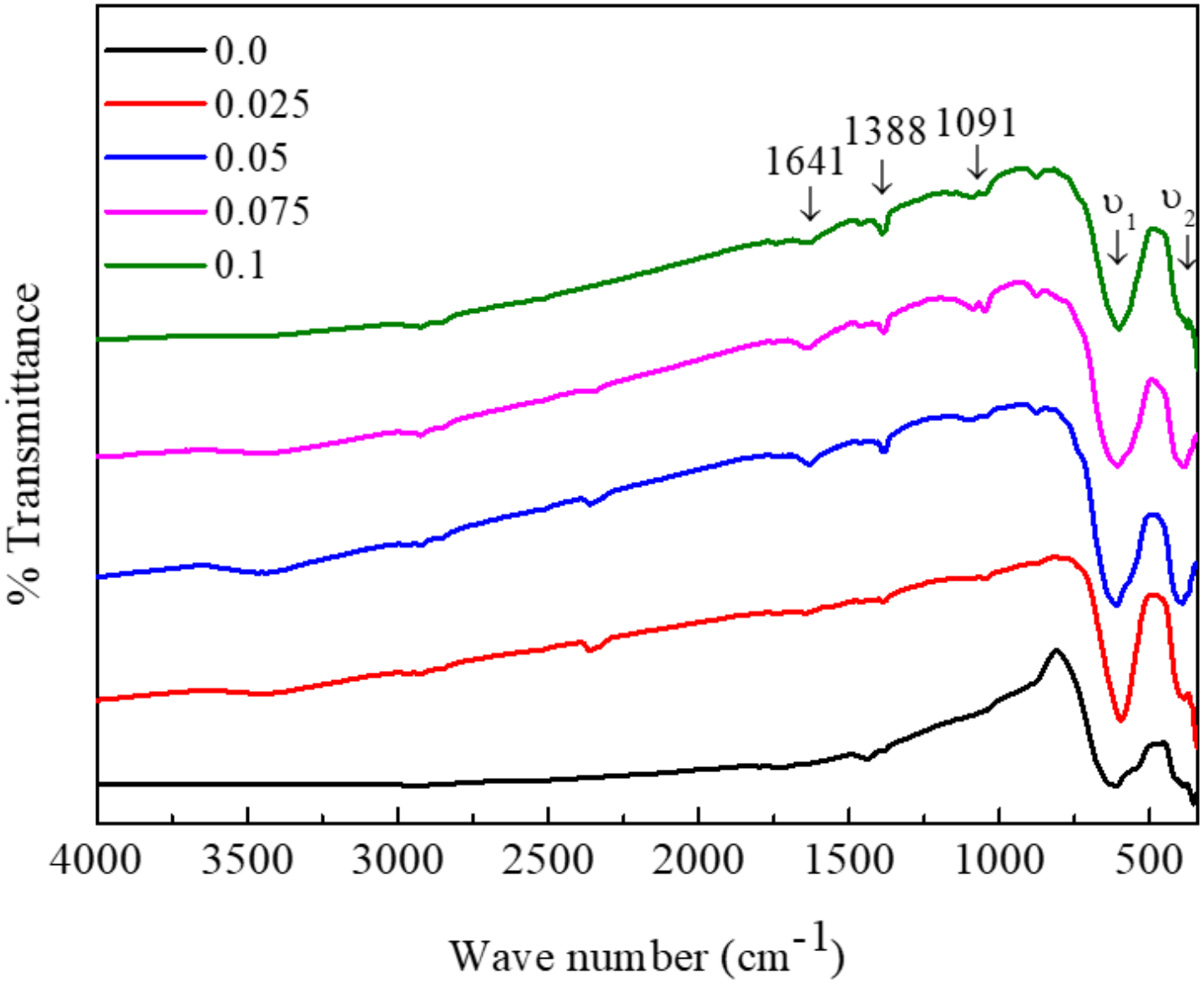

Figure 6

FTIR spectra of Ni0.2Ba0.1Co0.7Fe2-xSbxO4 (x=0, 0.025, 0.05, 0.075 and 0.1) nano ferrite.

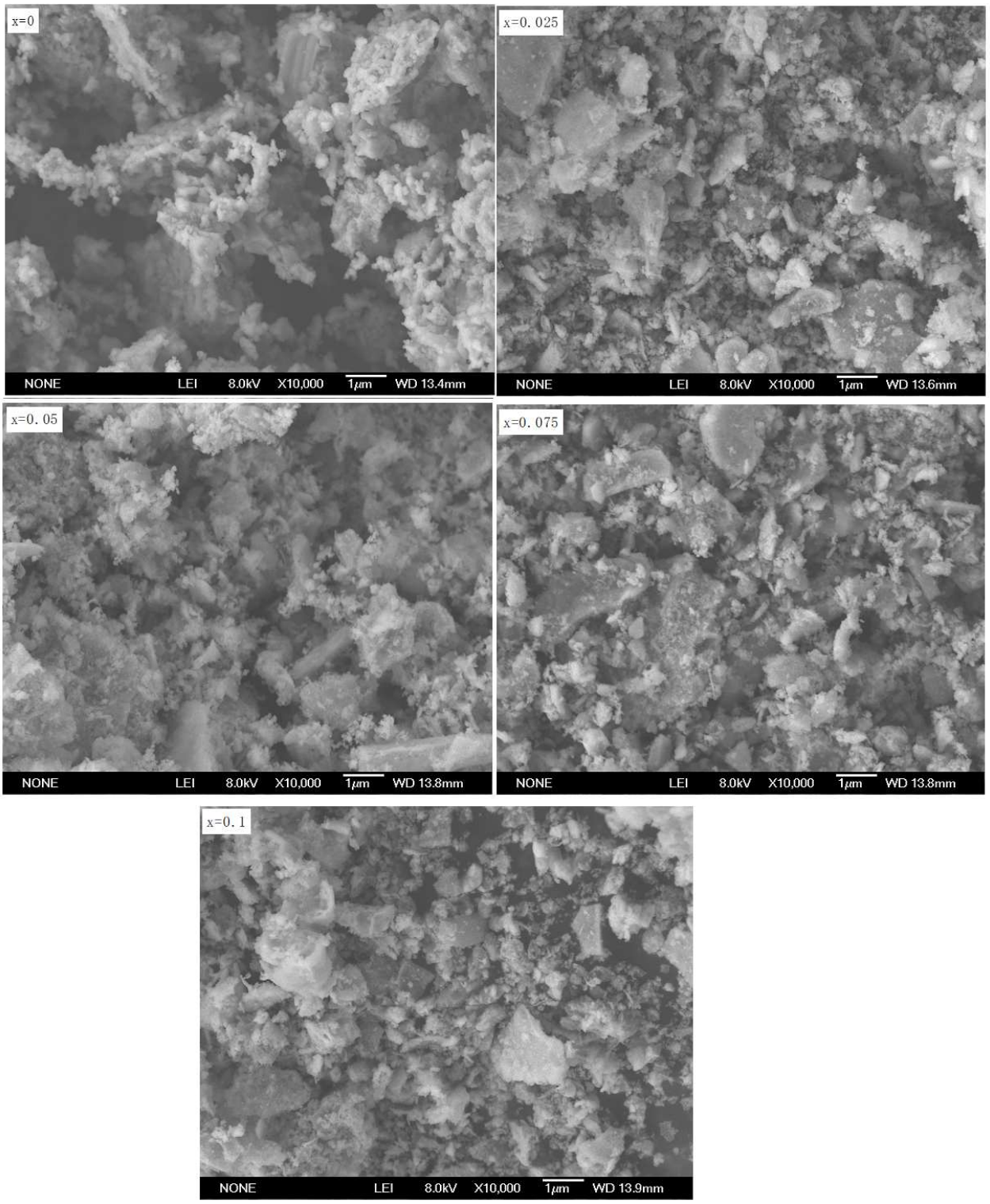

Figure 7

SEM micrographs of Ni0.2Ba0.1Co0.7Fe2-xSbxO4 (x=0, 0.025, 0.05, 0.075 and 0.1) nano ferrite.

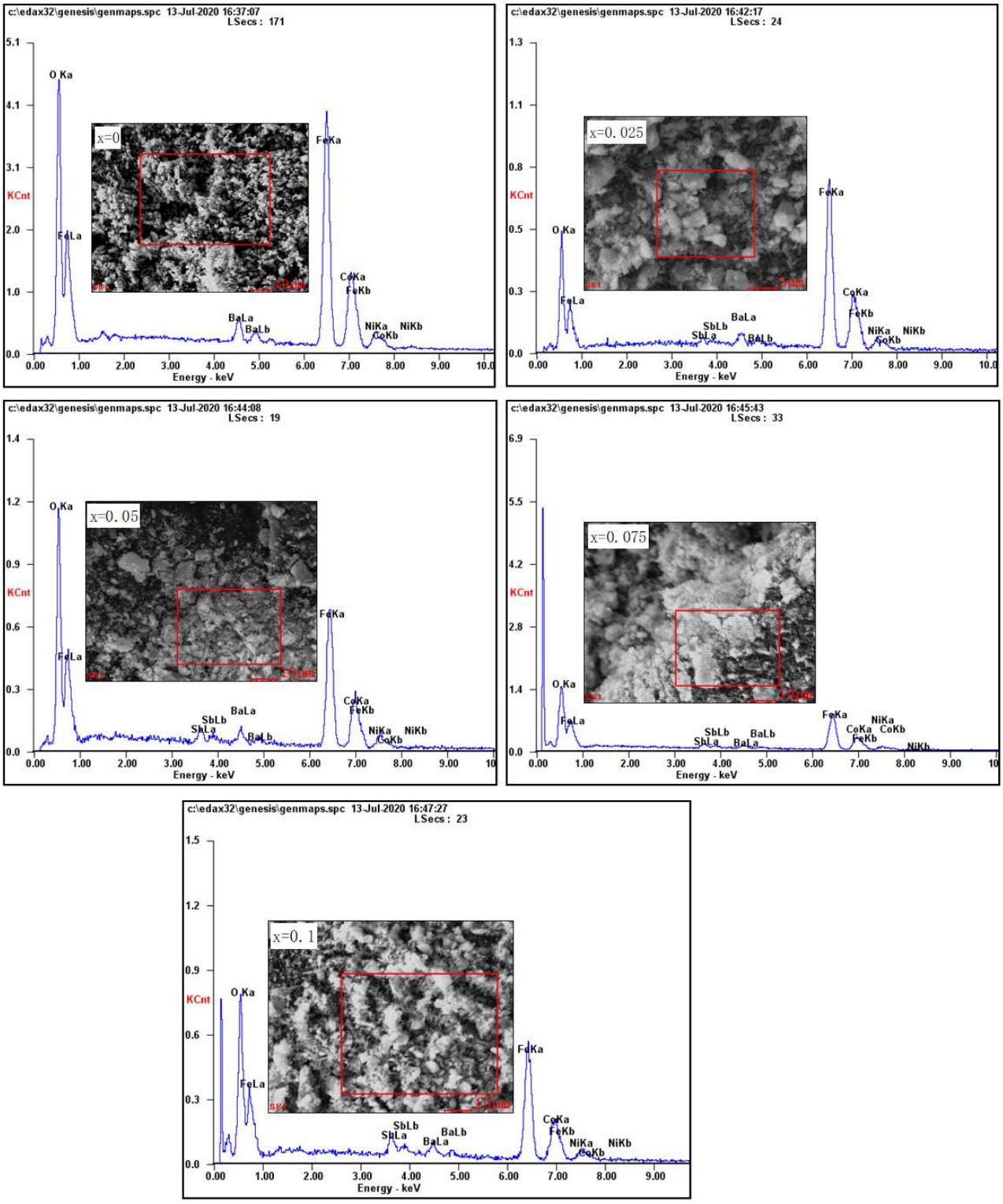

Figure 8

The EDS diagram of Ni0.2Ba0.1Co0.7Fe2-xSbxO4 (x=0, 0.025, 0.05, 0.075 and 0.1) nano ferrite.

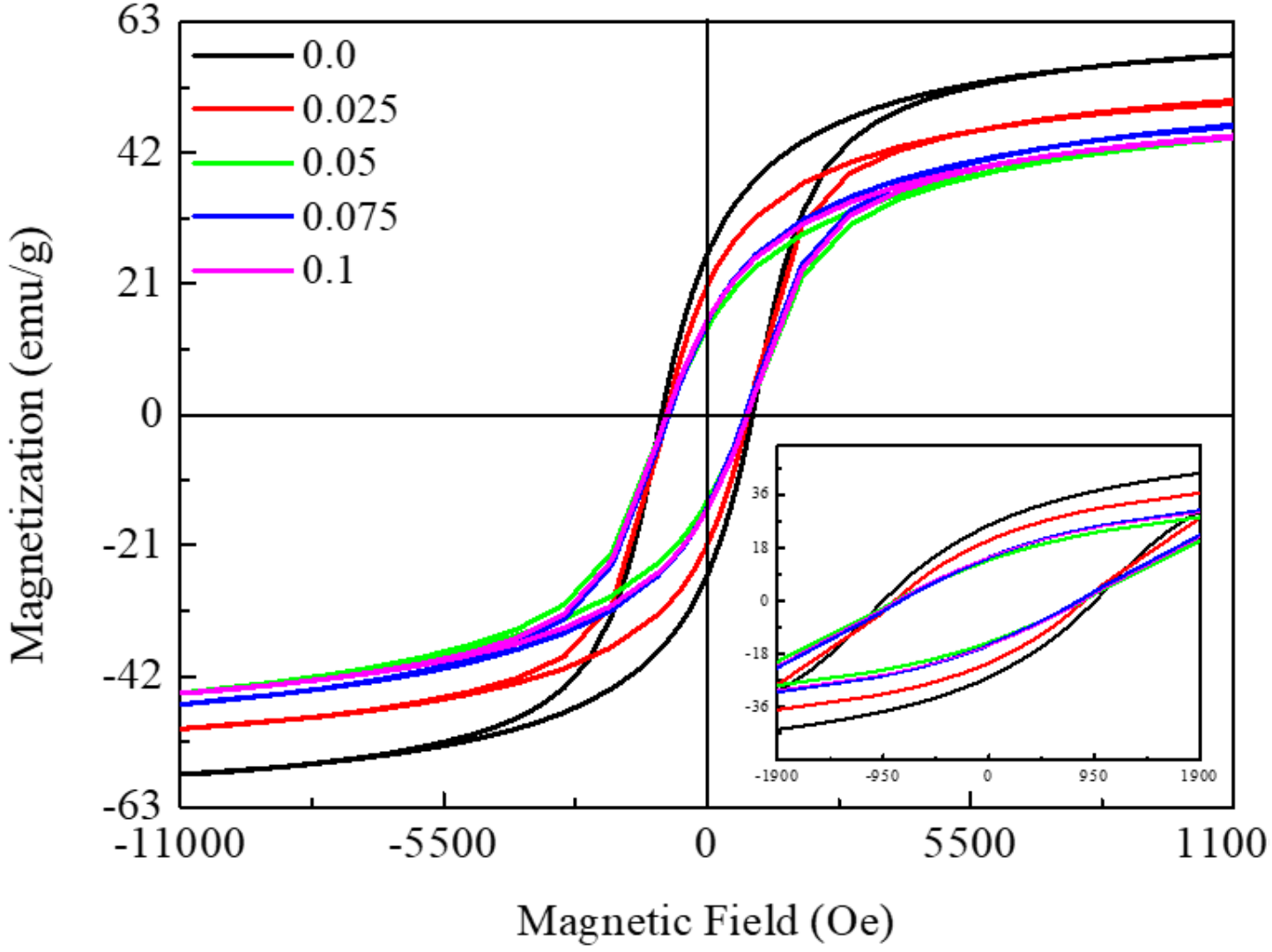

Figure 9

M-H Hysteresis loops of Ni0.2Ba0.1Co0.7Fe2-xSbxO4 (x=0, 0.025, 0.05, 0.075 and 0.1) nano ferrite.

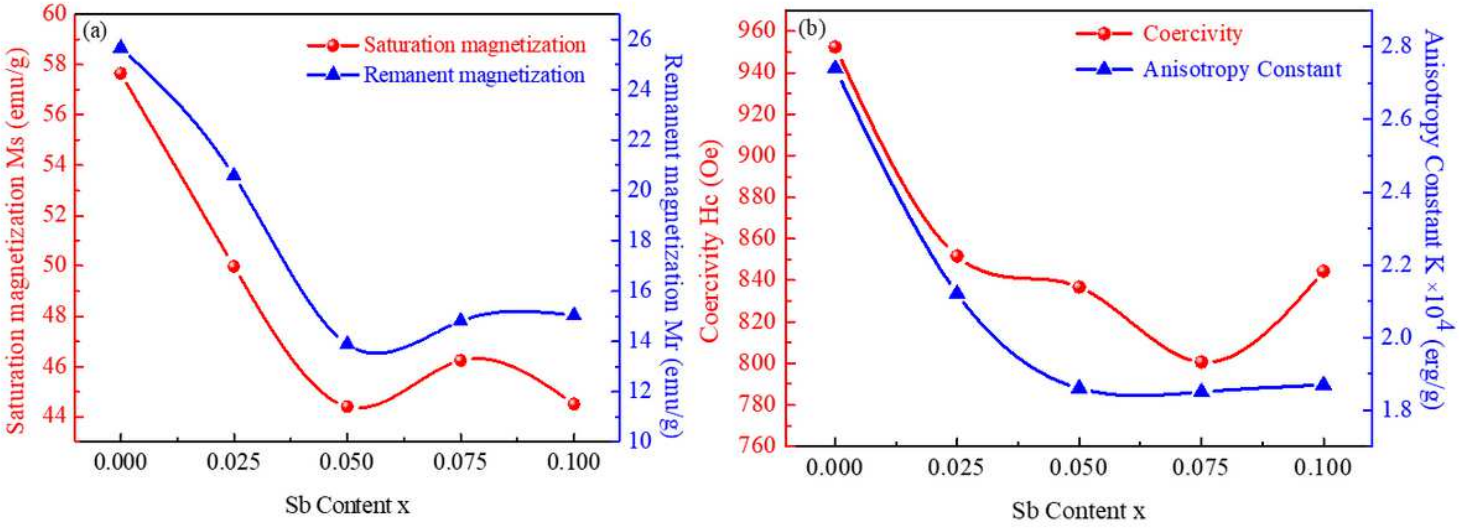

Figure 10

Variation of (a) saturation magnetization and remanent magnetization, (b) anisotropy constant and coercivity with Sb content x.

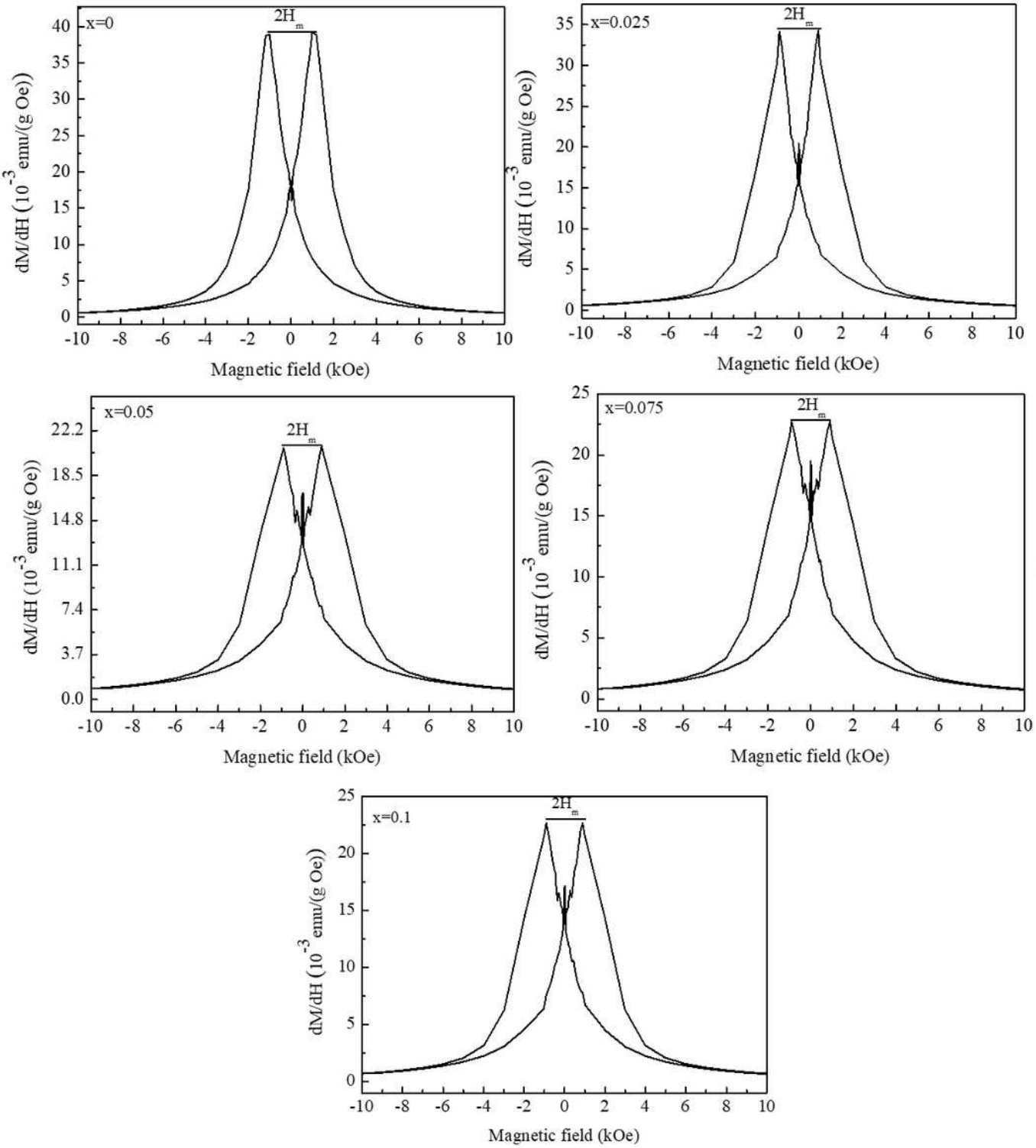

Figure 11

Field dependence of dM/dH of different samples. 2Hm measures the magnetic field that separates two peak.